

pubs.acs.org/macroletters Letter

Crossover from Rouse to Reptation Dynamics in Salt-Free Polyelectrolyte Complex Coacervates

Boyuan Yu, Phillip M. Rauscher, Nicholas E. Jackson, Artem M. Rumyantsev, and Juan J. de Pablo*



Cite This: ACS Macro Lett. 2020, 9, 1318-1324



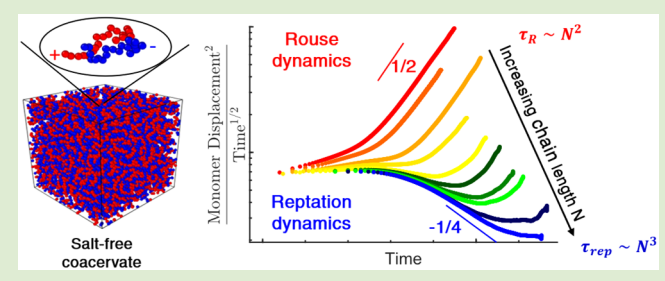
ACCESS

Metrics & More

Article Recommendations

Supporting Information

ABSTRACT: Considerable interest in the dynamics and rheology of polyelectrolyte complex coacervates has been motivated by their industrial application as viscosity modifiers. A central question is the extent to which classical Rouse and reptation models can be applied to systems where electrostatic interactions play a critical role on the thermodynamics. By relying on molecular simulations, we present a direct analysis of the crossover from Rouse to reptation dynamics in salt-free complex coacervates as a function of chain length. This crossover shifts to shorter chain lengths as electrostatic interactions become stronger, which corresponds to



the formation of denser coacervates. To distinguish the roles of Coulomb interactions and density, we compare the dynamics of coacervates to those of neutral, semidilute solutions at the same density. Both systems exhibit a universal dynamical behavior in the connectivity-dominated (subdiffusion and normal diffusion) regimes, but the monomer relaxation time in coacervates is much longer and increases with increasing Bjerrum length. This is similar to the cage effect observed in glass-forming polymers, but the local dynamical slowdown is caused here by strong Coulomb attractions (ion pairing) between oppositely charged monomers. Our findings provide a microscopic framework for the quantitative understanding of coacervate dynamics and rheology.

In solutions of oppositely charged polyelectrolytes (PEs), liquid—liquid phase separation can lead to the formation of a polymer-rich polyelectrolyte complex coacervate (PECC) phase in equilibrium with a polymer-lean supernatant phase. PECCs are used in a number of critical technologies as additives, rheology modifiers, 1,2 and drug delivery systems. 3,4 They are also believed to drive the formation of intracellular compartments that form the basis of biological systems. 5–8

The structure and rheology of PECCs have been characterized in a series of experimental studies. ^{9–14} In parallel, theoretical and computational efforts have gradually developed molecular-level descriptions of PECC thermodynamics and structure formation. ^{15,16} Little attention, however, has been directed toward the study of the dynamics and rheology of PECCs, and a comprehensive understanding of these aspects is still lacking.

The natural question is whether chain dynamics within PECCs can be described by classical Rouse and reptation models. ^{17,18} Aponte-Rivera and Rubinstein have argued that salt-free PECCs consisting of PEs, where only a small fraction of the monomers are charged, $f \ll 1$, can be treated as a melt of oppositely charged electrostatic blobs and are, therefore, similar to neutral semidilute solutions. ^{19–22} This view suggests that the Rouse and reptation models should be valid. ^{23,24} Consider salt-free symmetric PECC of flexible PEs containing N statistical segments, each of length a, in athermal solvent (Flory exponent $\nu = 0.588$). Each polyion is represented as a chain of N/g electrostatic blobs, and each blob contains $g \simeq$

 $(l_{\rm B}f^2/a)^{-1/(2-\nu)}$ monomers, $^{19-22}$ where $l_{\rm B}=e^2/\varepsilon k_{\rm B}T$ is the solvent Bjerrum length. The blob size, that is, the correlation length within the PECC, is written as $\xi\simeq ag^{\nu}\simeq a(l_{\rm B}f^2/a)^{-\nu/(2-\nu)}$. At $f\ll 1$, the Coulomb attraction between PEs is weak and ion pairing is negligible, 20,21 suggesting that the use of classical (nonsticky) models of polymer dynamics is appropriate. For short and long PEs, $N/g < N_{e0}$ and $N/g > N_{e0}$, chain dynamics can be described by the Rouse and reptation models, 17,18 respectively. Here N_{e0} is the number of monomers between adjacent entanglements in a melt, $N_{e0}\approx 30-50$. The chain relaxation time τ within the PECC then scales as 23,24

$$au_{
m R} \simeq au_{\xi} (N/g)^2 \qquad {
m for} \quad N/g < N_{e0} \ \simeq au_0 N^2 (l_{
m B} f^2/a)^{(2-3
u)/(2-
u)}$$

$$\begin{split} \tau_{\rm rep} &\simeq \tau_{\xi} (N/g)^3 N_{e0}^{-1} & \text{for } N/g > N_{e0} \\ &\simeq \tau_0 N^3 N_{e0}^{-1} (l_{\rm B} f^2/a)^{3(1-\nu)/(2-\nu)} & \end{split} \tag{1}$$

Received: July 17, 2020 Accepted: August 19, 2020 Published: August 26, 2020





where $\tau_{\xi} \simeq \eta_s \xi^3/k_{\rm B}T$ is the Zimm relaxation time of the blob, $\tau_0 \simeq \eta_s a^3/k_{\rm B}T$ is the monomer relaxation time, and η_s is the solvent viscosity. For highly charged PEs, $l_{\rm B} f^2/a \ge 1$, ionic pairs are formed between oppositely charged monomers, indicating that sticky Rouse and reptation models hould be applicable. In this case, τ_{ξ} and τ_0 in eq 1 should be modified to account for ion pairing, which slows down the local dynamics. I3,28,29

The theoretical prediction outlined above for the crossover from unentangled to entangled chain dynamics is consistent with recent experimental studies of PECC rheology. Schlenoff and co-workers systematically varied the molecular weight of PEs to reveal its effect on the storage $G'(\omega)$ and loss moduli $G''(\omega)$ of nearly salt-free PECCs. Theology was found to follow the predictions of the Rouse model: $G''(\omega)$ and $G'''(\omega)$ and $G'''(\omega)$ are at low frequencies, while at higher ω , these authors found $G'(\omega)$ at low frequencies, which at intermediate frequencies, which is a signature of entangled dynamics. PECC viscosity was observed to increase with chain length according to $\eta \sim N$ at low N, and as $\eta \sim N^{3.4}$ at high N, thereby supporting the existence of a dynamical crossover. The strength of the constraint of the co

The experimental and theoretical work described above can be supplemented by simulations in order to arrive at a detailed molecular view of the dynamical crossover in PECCs. Diddens et al. performed atomistic MD simulations of PE complexes, but the available time scales were not long enough to capture Rouse/reptation dynamics.²⁹ These simulations, however, did provide key insights into the local dynamics of the system. The authors reported, for example, that the effective dissociation of the ion pair, accompanied by the change of the pairing partner and microscopic rearrangement, is preceded by multiple elementary dissociation and recombination events without a change of partner. This result supports the renormalization of the ion pair lifetime²⁹ that is implicit in sticky dynamics models.^{26,27} Coarse-grained simulations of PECC dynamics have also been presented, 30 but with an emphasis on calculating the dynamical modulus and exploring whether salt-time superposition arises in model systems. For the chain lengths considered in that study, the resulting PECC rheology appeared to be Rouse-like.³⁰

Building on these previous studies, in this work we rely on simulations of a coarse-grained (CG) polymer model to directly analyze the Rouse to reptation dynamical crossover in PECCs. By tracking the microscopic diffusion of PE monomers within the PECC, we observe the dynamical crossover as a function of several critical system parameters. Specifically, we focus our analysis on the influence of chain length, and on the effects of Coulomb interaction strength on the transition between the Rouse and reptation regimes.

The Kremer-Grest model,³¹ augmented with electrostatic interactions, is adopted here, with the solvent represented as a continuum with dielectric constant ϵ . All systems contain an equal number of fully charged polycations and polyanions of identical chain length, N, thereby preserving electroneutrality. Chain lengths are varied between N=15 and 500, and system sizes range from 15000 to 120000 total beads. Counterions are omitted, since in this first study we are interested in salt-free PECCs. We consider Bjerrum lengths of $l_{\rm B}/\sigma=1/3,\,1,\,3,\,6,\,8$, and 10. To prepare the dense coacervate phase, the system is maintained at an osmotic pressure p=0. Constant temperature and the effects of solvent fluctuations are introduced through

the use of a Langevin thermostat. Since the solvent is represented implicitly, the bead number density, ρ , is effectively synonymous with the polymer volume fraction, that is, $\phi \simeq \rho \sigma^3$, and the two are used somewhat interchangeably throughout this Letter. Throughout this work, the characteristic units for distance and time are the Lennard-Jones (LJ) bead diameter, σ , and the LJ unit of time, $\tau_{\rm LJ} = (m\sigma^2/k_{\rm B}T)^{1/2}$, respectively, where m is the bead mass. Additional details can be found in the Supporting Information.

To access the long time scales required to observe entangled polymer dynamics, we have adopted a model that neglects hydrodynamic interactions (HI). This approximation is justified on the basis that HI does not influence the onset of chain entanglement at equilibrium, as this transition reflects structural features of the solution. The absence of HI does not influence the crossover from Rouse to reptation dynamics, and it allows us to extend our simulations to the time scales that are necessary to observe diffusion in entangled materials. Also note that, in experiments, HI within PECCs are screened and can be neglected beyond lengths that exceed the correlation length ξ . The dynamics should therefore be universal for $t > \tau_{\varepsilon_t}$ making our simulations applicable to experimental systems. In the absence of HI, the relaxation times can be estimated by eq 1, but taking the blob relaxation time τ_{ξ} as the Rouse (rather than Zimm) time, given by $\tau_{\varepsilon} \simeq \xi^2/D \simeq \tau_0 g^{1+2\nu}$, since the Rouse diffusion coefficient $D \simeq k_{\rm B}T/g\eta_{\rm s}a^{17}$ The relaxation times then

$$\begin{split} \tau_{\rm R} &\simeq \tau_0 N^2 (l_{\rm B} f^2/a)^{-(2\nu-1)/(2-\nu)} & \text{for } N/g < N_{e0} \\ &\simeq \tau_0 N^2 \phi^{-(2\nu-1)/(3\nu-1)} \\ \tau_{\rm rep} &\simeq \tau_0 N^3 N_{e0}^{-1} (l_{\rm B} f^2/a)^{2(1-\nu)/(2-\nu)} & \text{for } N/g > N_{e0} \\ &\simeq \tau_0 N^3 N_{e0}^{-1} \phi^{2(1-\nu)/(3\nu-1)} \end{split}$$

To establish the existence of the dynamical crossover and determine the influence of $l_{\rm B}$ on the crossover chain length N_e , we begin by conducting simulations for $l_{\rm B}/\sigma=1/3$, 1, and 3, and characterize the dynamics through the MSD of the central five monomers $\langle \Delta R^2(t) \rangle$ often denoted $g_1(t)^{31}$ versus time t. For semidilute solutions in athermal solvent, the classical Rouse model predicts the existence of two scaling regimes at time scales exceeding the blob relaxation time τ_{ε} : 18

$$\langle \Delta R^2(t) \rangle \sim \begin{cases} t^{1/2} & \text{for } \tau_{\xi} < t < \tau_{R} \\ t & \text{for } \tau_{R} < t \end{cases}$$
 (3)

Here $\tau_R \simeq \tau_{\xi} (N/g)^2$ is the Rouse relaxation time of the chain. For entangled solutions, four different regimes can be identified: 17

$$\langle \Delta R^{2}(t) \rangle \sim \begin{cases} t^{1/2} & \text{for } \tau_{\xi} < t < \tau_{e} \\ t^{1/4} & \text{for } \tau_{e} < t < \tau_{R} \end{cases}$$
$$t^{1/2} & \text{for } \tau_{R} < t < \tau_{rep} \\ t & \text{for } \tau_{rep} < t \end{cases}$$
(4)

where $\tau_e \simeq \tau_\xi N_{e0}^2$ is the Rouse relaxation time of an entanglement strand containing $N_e \simeq g N_{e0}$ monomers, and $\tau_{\rm rep} \simeq \tau_e (N/g N_{e0})^3$ is the reptation time needed for tube renewal.

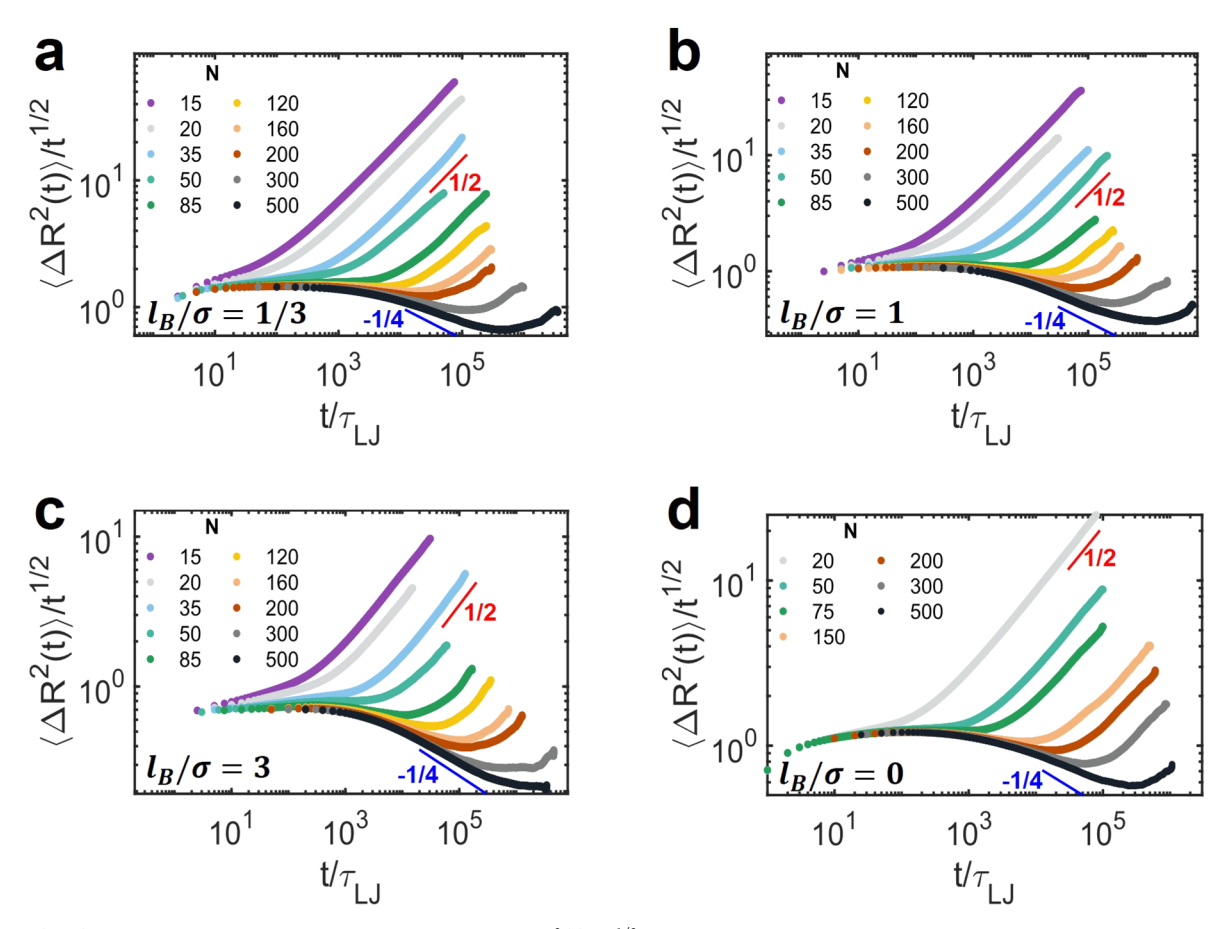


Figure 1. (a-c) Log-log plots for the time-normalized MSD $\langle \Delta R^2(t) \rangle / t^{1/2}$ as a function of t for a set of chain lengths N and Bjerrum lengths $l_{\rm B}/\sigma$ equal to (a) 1/3, (b) 1, and (c) 3. (d) The same plot for the neutral system, $l_{\rm B}=0$ at the density of 0.45 σ^{-3} , which is equal to the coacervate equilibrium density at $l_{\rm B}/\sigma=3$.

It is convenient to "normalize" the MSD on the basis of the Rouse theory prediction, namely, $\langle \Delta R^2(t) \rangle / t^{1/2}$, so that for unentangled dynamics this quantity becomes constant at times $\tau_\xi < t < \tau_R$. When viewed on a log-log scale, the slope of this quantity should transition from 0 to 1/2 at τ_R for small N with no other dynamical regimes. However, for long entangled chains with $N > N_e$, the slope should decrease from 0 to -1/4, and later increase to 0 and then to 1/2, according to the predictions of eq 4.

The anticipated changes in $\langle \Delta R^2(t) \rangle / t^{1/2}$ versus t, which reflect the underlying dynamical crossover, are apparent in Figure 1a—c for all three $l_{\rm B}$ values. For instance, in Figure 1c, the slope changes from 0 to 1/2 at $N \leq 50$, in accordance with the Rouse model predictions given by eq 3. For N > 50, the slope is equal to 0 at low t and then decreases at longer times in a manifestation of entanglement dynamics. For N = 300, all four regimes of eq 4 are clearly observed. The results shown in Figure 1a—c provide compelling evidence of a crossover from Rouse to reptation dynamics in PECCs as chain length is increased.

A comparison of Figure 1a—c shows that the dynamical crossover takes place at lower N values as the strength of Coulomb interactions, that is, $l_{\rm B}$, increases. This is due to a higher coacervate density ϕ and a lower correlation length ξ at high $l_{\rm B}$. This trend can be qualitatively understood from the scaling estimate for the threshold PE length, independent of HI (see discussion before eq 1):

$$N_e \simeq gN_{e0} \simeq (l_B f^2/a)^{-1/(2-\nu)} N_{e0}$$
 (5)

This scaling result captures the trend of decreasing N_e with increasing $l_{\rm B}$, $N_e \sim l_{\rm B}^{-0.71}$, in athermal solvent. Note, however, that it should only hold rigorously for weakly charged PEs^{20,21} with $l_{\rm B}f^2/a \ll 1$, whereas our simulations consider fully charged chains.

The dynamic crossover can also be examined through the dependence of the longest relaxation time τ on chain length N. Specifically, eq 1 predicts $\tau \sim N^2$ and $\tau \sim N^3$, in the respective scaling regimes. The averaged relaxation time $\langle \tau \rangle$ can be determined from the end-to-end vector autocorrelation function (see Figure S2). The dependence of $\langle \tau \rangle$ on chain length N for $l_B/\sigma = 1/3$, 1, and 3 is shown in Figure 2 a-c, respectively. For all $l_{\rm B}$ values, $\langle \tau \rangle$ exhibits different scaling with N for short and long chains. At high N, $\langle \tau \rangle \sim N^3$, as expected for entangled dynamics (see blue dashed lines in Figures 2a-c and S3). At low N, where PE chains exhibit Rouse dynamics, the exponent in this scaling law is considerably lower than 3 (red dashed lines). These results further demonstrate the crossover from Rouse to reptation dynamics in PECC at increasing PE length. One also observes that the crossover chain length N_{e} denoted by the magenta stars in Figure 2a-c, decreases as $l_{\rm B}$ grows, consistent with the results of the MSD analysis of Figure 1.

Note that the calculated relaxation times for short chains deviate from the theoretically expected Rouse scaling $\langle \tau \rangle \sim N^2$; Figure 2a–c shows that the apparent exponent is around 2.5.

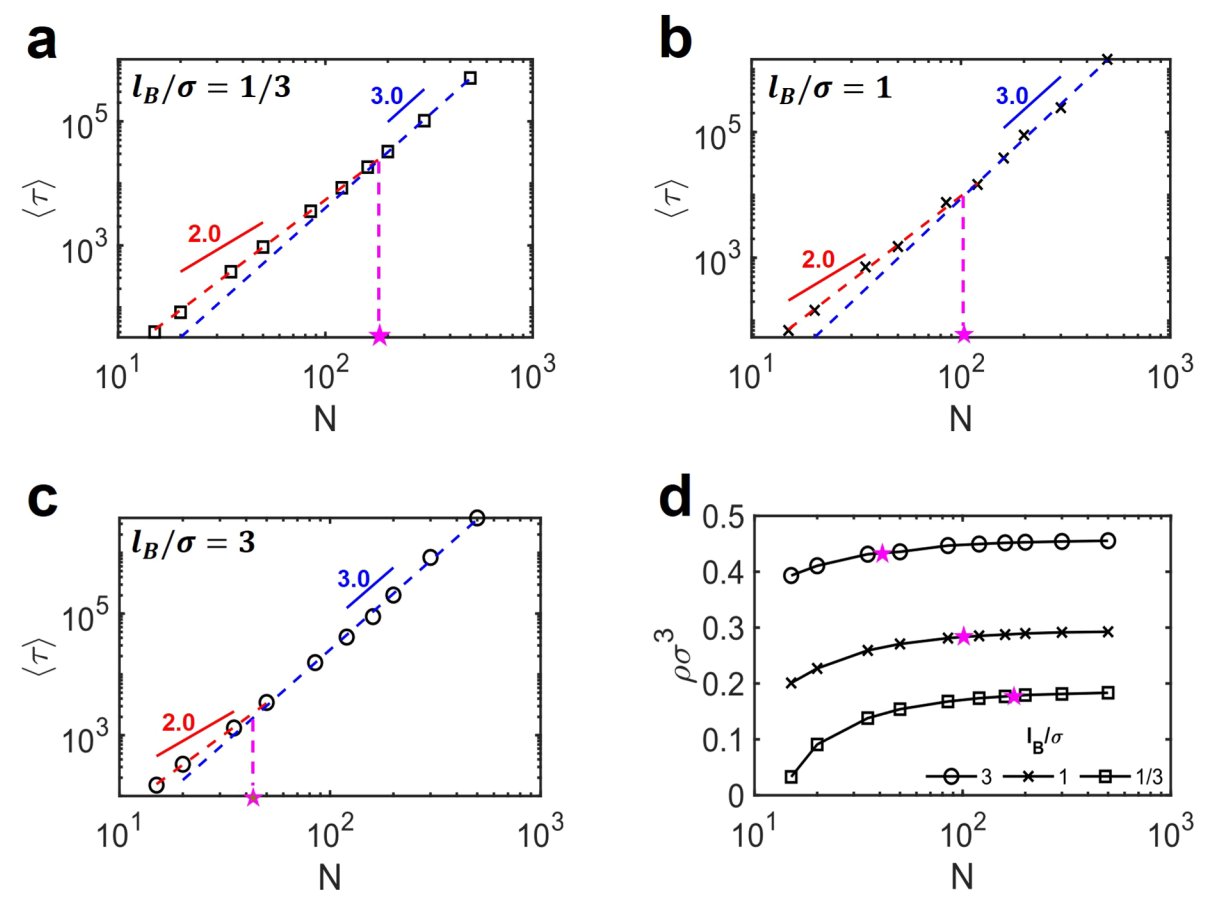


Figure 2. (a-c) Relaxation time $\langle \tau \rangle$ vs chain length N for different l_B/σ equal to (a) 1/3, (b) 1, (c) 3. Confidence intervals of 95% are comparable to the size of the data points. Red and blue dashed lines represent fits to simulation data in the regions of low and high N, corresponding to unentangled and entangled dynamics, respectively. The crossover between these regimes is denoted by a magenta star. (d) Corresponding equilibrium density of salt-free PECC as a function of chain length N. The star symbols show the position of the dynamical crossover from (a)—(c).

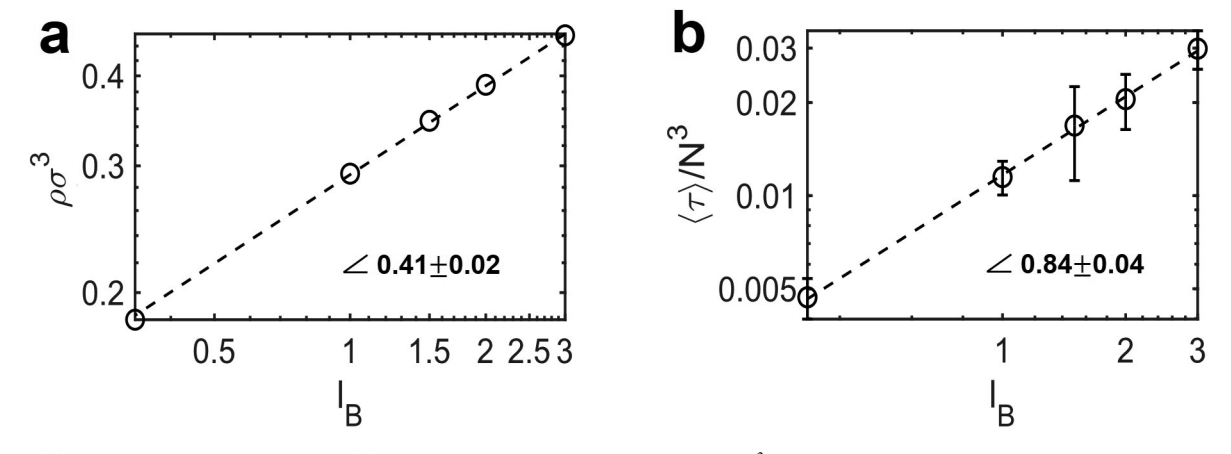


Figure 3. (a) PECC number density ρ and (b) length-normalized relaxation time $\langle \tau \rangle/N^3$ as the functions of Bjerrum length $l_{\rm B}$ for N=500. Power law fits are shown in dashed lines along with apparent exponents with 95% confidence intervals.

We believe that the main reason for this discrepancy is the dependence of the equilibrium PECC number density ρ on chain length in the range of low N, where dynamics is Rouselike. In Figure 2d, one observes that the density is an increasing function of N that levels off at sufficiently high N, when PE translational entropy becomes negligible. It appears that the density saturation and the position of the dynamical crossover denoted by magenta stars coincide. For this reason, the expected scaling exponent 3 is observed in the reptation regime

at $N > N_e$, while in the Rouse regime the relaxation time increases with N more rapidly than expected theoretically. The latter is due to the increasing coacervate density that accompanies the chain length growth at $N < N_e$ (recall that eqs 1 and 2 assume PECC density to be independent of N). The higher the PECC density, the larger the number of contacts between monomers, and the greater the effective monomeric friction. These effects may be exacerbated by the electrostatic interactions that can cause ion-pairing at high $l_{\rm R}$,

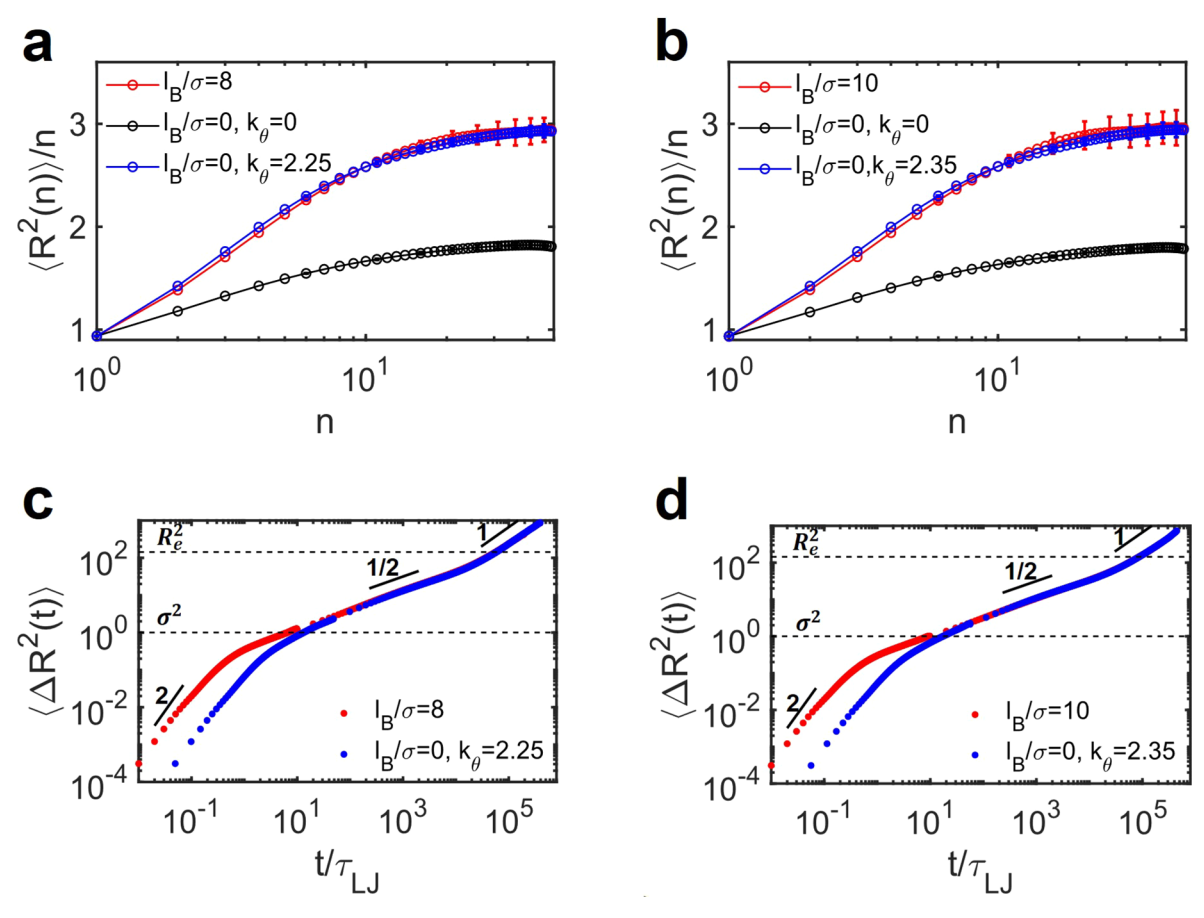


Figure 4. (a, b) Mean-squared internal distances of PE chains (red) of length N = 50 in PECCs for $l_{\rm B}/\sigma$ equal to (a) 8 and (b) 10 and for neutral chains without (black) and with (blue) angle potential at same densities (a) $\rho\sigma^3 = 0.63$ and (b) $\rho\sigma^3 = 0.69$. (c, d) The MSD of the central five monomers of PE chains in PECCs (red) for $l_{\rm B}/\sigma$ equal to (c) 8 and (d) 10 and the corresponding neutral chains with angle potentials (blue). Curves for neutral chains are shifted to the right by a factor of (c) 4.6 and (d) 5.6 to coincide with those of PEs. Dashed lines show the MSD equal to the monomer size σ^2 and to the chain end-to-end distances R_c^2 .

leading to Rouse dynamics with a renormalized friction coefficient.²⁶ In contrast, a scaling exponent of 2 in the low-*N* regime is clearly observed in neutral semidilute solutions at constant density (see Figure S4).

Since in the regime of entangled dynamics the scaling law τ $\sim N^3$ is fulfilled, one can examine the dependence of $\langle \tau \rangle / N^3$ on $l_{\rm B}$ to reveal the effect of Coulomb interaction strength on the PECC relaxation times. The corresponding dependence calculated for the longest chains, N = 500, is shown in Figure 3b, and the exponent in the scaling law $\langle \tau \rangle \sim l_B^x$ is equal to x = 0.84 ± 0.04 . This result differs from the scaling estimates given by eq 2 predicting $x = 2(1 - \nu)/(2 - \nu) = 0.58$ for athermal solvent. The disagreement is actually even stronger than it appears. The blob picture assumes weakly charged chains with $l_{\rm B}f^2/a \ll 1$ and, hence, low density, $\phi \ll 1$, 20,21 while in simulations, we deal with fully charged PEs that do not obey these requirements (see also Figure S5). Indeed, the scaling picture of PECC^{19,21} implies $\phi \simeq ga^3/\xi^3 \simeq (l_B f^2/a)^{(3\nu-1)/(2-\nu)}$ $\sim l_{\rm B}^{0.54}$, while simulation data shown in Figure 3a yields a lower slope of 0.41 ± 0.02 owing to the lower compressibility at high density. Combining the observed scaling law for ϕ with the dependence of the relaxation time on density provided by eq 2, $au_{\rm rep} \sim \phi^{1.08}$, we arrive at $au_{\rm rep} \sim l_{\rm B}^{0.44}$. Thus, the observed scaling for $\langle au \rangle$ versus $l_{\rm B}$ (Figure 3b) is much faster than that expected theoretically. This discrepancy suggests that the monomeric

relaxation time τ_0 (or the effective friction), which was assumed to be constant above, actually increases with $l_{\rm B}$.

The observations above can be rationalized by density effects and electrostatics, which couple to modify the effective friction in our simulations, as mentioned earlier. The faster scaling of $\langle \tau \rangle$ with $l_{\rm B}$ is directly related to these same factors. To recapitulate, changes in the density lead to more frequent bead—bead interactions, effectively increasing the friction even in neutral systems. Since the density depends strongly on $l_{\rm B}$, so too will the effective friction. Additionally, even at the fixed density, increases in $l_{\rm B}$ enhance electrostatic interactions and can lead to ion pairing, further increasing bead relaxation times. At high $l_{\rm B}$, electrostatic stiffening of PEs 33,34 is the additional effect neglected in the scaling analysis. In light of these considerations, it is not surprising that $\langle \tau \rangle$ scales with $l_{\rm B}$ more quickly than expected from on-blob arguments.

Additional information on the influence of electrostatic interactions on the dynamics of PECCs can be extracted by comparing results for charged and neutral chains at the highest studied $l_{\rm B}$, where the effect of Coulomb interactions on dynamics is the strongest, at the same density. There is a challenge associated with the inherent difference between conformational statistics for PECCs and neutral polymers, even at the same density. Neutral chains in solution are more flexible than the charged chains in PECCs due to the electrostatic stiffening of the PEs. 33,34 This effect is clearly

seen in the mean-squared internal distances, $\langle R^2(n)\rangle/n$ (Figure 4a,b), which track the average distance between monomers separated by n bonds.³⁵ To generate similar statistics for neutral chains in solution and for PEs in PECCs, we introduce a local three-body angle potential between neutral monomers of the form $U(\theta)/(k_{\rm B}T)=k_{\theta}(1+\cos\theta)$. Figure 4a,b show that the angle coefficients required to enforce equivalent statistics are approximately $k_{\theta}=2.25$ for $l_{\rm B}/\sigma=8$ and $k_{\theta}=2.35$ for $l_{\rm B}/\sigma=10$. The higher the Bjerrum length $l_{\rm B}$, the higher the effective PE stiffness, that is, the larger the effective bond length (equal to the square root of the plateau value of $\langle R^2(n)\rangle/n$ in Figure 4a,b), and the higher the corresponding k_{θ} value in the neutral solution. The same trend is observed for not only N=50, but also N=20, see Figure S6.

Figure 4c,d shows the MSD of monomers within PECCs at $l_{\rm B}/\sigma = 8$ and 10, respectively, for N = 50, when chains exhibit Rouse dynamics. These plots also present the MSD for the corresponding neutral solutions, which were time-shifted to collapse all curves onto the same master curve in the diffusion regime. The time shift factors, equal to 4.6 and 5.6 for $l_{\rm B}/\sigma=8$ and 10, respectively, quantify the dynamical slow down induced by Coulomb interactions. It is uniformly observed that higher $l_{\rm B}$ values lead to slower local dynamics. Time shift factors are equal to the decrease of the chain diffusion coefficient (or, equivalently, to the increase in the effective friction coefficient of the entire chain) relative to neutral solutions with identical chain statistics. An analogous increase in the effective friction caused by Coulomb interactions between charged monomers and counterions was observed in concentrated PE solutions.36

For the large Bjerrum lengths considered in Figure 4, PECC density is also high ($\rho\sigma^3=0.69$) and becomes comparable to the density of the melt, that is, $\xi\simeq\sigma$, and the relaxation times of the blob and monomer are nearly equal. Figure 4c,d demonstrate that three different regimes of monomer diffusion can be distinguished for both PECCs and neutral solutions. At very short times, $t\ll\tau_\xi$, a ballistic regime with $\Delta R^2(t)\sim t^2$ can be identified. It is followed by the connectivity-dominated subdiffusion outside of the correlation volume with $\Delta R^2(t)\sim t^{1/2}$. The regime corresponding to subdiffusion within the blob, with $\sigma^2<\Delta R^2(t)<\xi^2$, where hydrodynamic and excluded volume interactions are important, is practically absent at high $l_{\rm B}$ because $\xi\simeq\sigma$. The subdiffusive regime occurs for $\tau_\xi< t<\tau_{\rm R}$ and is followed by regular diffusion at $t>\tau_{\rm R}$. For PECCs, the Rouse relaxation time of the chain increases with increasing $l_{\rm B}$.

We note that the curves for the PECC and the corresponding neutral solution coincide not only in the normal diffusive regime, but also in the subdiffusive regime. For each $l_{\rm B}$, the corresponding time shift factor is also equal to the ratio of the chain relaxation time in the PECC and in the neutral solution. Thus, for the highest $l_{\rm B}$ considered here, our data illustrate the applicability of the Rouse model with renormalized monomer friction to unentangled chain dynamics in dense PECCs. One should just substitute the monomer relaxation time in the corresponding concentrated solution of a neutral polymer, τ_0 (which is controlled by free diffusion), with the effective monomer relaxation time τ_0^* accounting for the slowdown induced by Coulomb interactions (ion pairing).²⁹ The ratio between these times, τ_0^*/τ_0 , is equal to the corresponding time shift factors discussed above.

This dynamical slowdown in dense PECCs (with respect to neutral solutions) is very similar to that in polymer melts in the glass transition region. Strong Coulomb interactions in

PECCs and caging effects in glasses^{37–39} serve to slow the local dynamics, but the effective Rouse behavior is retained at longer time scales as a consequence of the monomers' connectivity. We also expect that PECCs comprising longer chains will form entanglements and exhibit reptation behavior.²⁷ However, the change in the monomer relaxation time due to Coulomb interactions, $\tau_0 \rightarrow \tau_0^*$, should be independent of N.

Taken together, the results of coarse-grained simulations for various dynamical properties demonstrate the existence of a crossover from unentangled to entangled dynamics with increasing molecular weight in salt-free coacervates. Our results also show that the reptation model can be applied to PEs with shorter chain lengths as $l_{\rm B}$ increases, which qualitatively coincides with the predictions from scaling theory. When compared to that for neutral polymers, as a result of electrostatic interactions, the chain relaxation time of polymers in PECCs is much slower. When differences in conformational statistics and densities are accounted for, the chain relaxation times and MSD of monomers in the normal diffusion regime differ by a factor of 5 at $l_{\rm B}/\sigma=10$, and this factor increases with increasing Bjerrum length. Our findings serve to clarify the effects of electrostatics on charged polymer dynamics and help provide a foundation to build a better understanding of coacervate dynamics and rheology.

ASSOCIATED CONTENT

3 Supporting Information

The Supporting Information is available free of charge at https://pubs.acs.org/doi/10.1021/acsmacrolett.0c00522.

(1) Simulation details and structural characterization of the polymers; (2) Additional figures; (3) Scaling estimates for relaxation times of PEs within PECCs in athermal and θ solvents with and without hydrodynamic interactions.

AUTHOR INFORMATION

Corresponding Author

Juan J. de Pablo — Pritzker School of Molecular Engineering, University of Chicago, Chicago, Illinois 60637, United States; Center for Molecular Engineering and Materials Science Division, Argonne National Laboratory, Lemont, Illinois 60439, United States; ⊙ orcid.org/0000-0002-3526-516X; Email: depablo@uchicago.edu

Authors

Boyuan Yu — Pritzker School of Molecular Engineering, University of Chicago, Chicago, Illinois 60637, United States; orcid.org/0000-0002-8200-4413

Phillip M. Rauscher — Pritzker School of Molecular Engineering, University of Chicago, Chicago, Illinois 60637, United States; Occid.org/0000-0002-0441-6439

Nicholas E. Jackson — Pritzker School of Molecular Engineering, University of Chicago, Chicago, Illinois 60637, United States; Center for Molecular Engineering and Materials Science Division, Argonne National Laboratory, Lemont, Illinois 60439, United States; Occid.org/0000-0002-1470-1903

Artem M. Rumyantsev — Pritzker School of Molecular Engineering, University of Chicago, Chicago, Illinois 60637, United States; o orcid.org/0000-0002-0339-2375

Complete contact information is available at: https://pubs.acs.org/10.1021/acsmacrolett.0c00522

Notes

The authors declare no competing financial interest.

ACKNOWLEDGMENTS

We benefited from a collaboration with Heyi Liang. A.M.R. thanks Jörg Baschnagel and Albert Johner for valuable discussions. Computing resources were provided by the Laboratory Computing Resource Center (LCRC) at Argonne National Laboratory and the University of Chicago Research Computing Center (RCC). This work is supported by the Department of Energy, Office of Science, Basic Energy Sciences, Materials Science and Engineering Division. The simulations reported here were carried out on the GPU cluster supported by the NSF through Grant DMR-1828629.

REFERENCES

- (1) Schmitt, C.; Turgeon, S. L. Protein/polysaccharide complexes and coacervates in food systems. *Adv. Colloid Interface Sci.* **2011**, *167*, 63–70.
- (2) Kalantar, T.; Tucker, C.; Zalusky, A.; Boomgaard, T.; Wilson, B.; Ladika, M.; Jordan, S.; Li, W.; Zhang, X.; Goh, C. High throuhgput workflow for coacervate formation and characterization in shampoo systems. *J. Cosmet. Sci.* **2007**, *58*, 375–384.
- (3) Black, K. A.; Priftis, D.; Perry, S. L.; Yip, J.; Byun, W. Y.; Tirrell, M. Protein encapsulation via polypeptide complex coacervation. *ACS Macro Lett.* **2014**, *3*, 1088–1091.
- (4) Acar, H.; Ting, J. M.; Srivastava, S.; LaBelle, J. L.; Tirrell, M. V. Molecular engineering solutions for therapeutic peptide delivery. *Chem. Soc. Rev.* **2017**, *46*, 6553–6569.
- (5) Hyman, A. A.; Simons, K. Beyond oil and water—phase transitions in cells. *Science* **2012**, 337, 1047–1049.
- (6) Aumiller, W. M., Jr; Keating, C. D. Phosphorylation-mediated RNA/peptide complex coacervation as a model for intracellular liquid organelles. *Nat. Chem.* **2016**, *8*, 129–137.
- (7) Shin, Y.; Brangwynne, C. P. Liquid phase condensation in cell physiology and disease. *Science* **2017**, *357*, eaaf4382.
- (8) Perry, S. L. Phase separation: Bridging polymer physics and biology. Curr. Opin. Colloid Interface Sci. 2019, 39, 86-97.
- (9) Spruijt, E.; Sprakel, J.; Lemmers, M.; Cohen Stuart, M. A.; van der Gucht, J. Relaxation dynamics at different time scales in electrostatic complexes: Time-salt superposition. *Phys. Rev. Lett.* **2010**, *105*, 208301.
- (10) Spruijt, E.; Cohen Stuart, M. A.; van der Gucht, J. Linear viscoelasticity of polyelectrolyte complex coacervates. *Macromolecules* **2013**, *46*, 1633–1641.
- (11) Liu, Y.; Winter, H. H.; Perry, S. L. Linear viscoelasticity of complex coacervates. *Adv. Colloid Interface Sci.* **2017**, 239, 46–60.
- (12) Marciel, A. B.; Srivastava, S.; Tirrell, M. V. Structure and rheology of polyelectrolyte complex coacervates. *Soft Matter* **2018**, *14*, 2454–2464.
- (13) Yang, M.; Shi, J.; Schlenoff, J. B. Control of dynamics in polyelectrolyte complexes by temperature and salt. *Macromolecules* **2019**, *52*, 1930–1941.
- (14) Akkaoui, K.; Yang, M.; Digby, Z. A.; Schlenoff, J. B. Ultraviscosity in entangled polyelectrolyte complexes and coacervates. *Macromolecules* **2020**, 53, 4234.
- (15) Sing, C. E. Development of the modern theory of polymeric complex coacervation. *Adv. Colloid Interface Sci.* **2017**, 239, 2–16.
- (16) Sing, C. E.; Perry, S. L. Recent progress in the science of complex coacervation. *Soft Matter* **2020**, *16*, 2885–2914.
- (17) Doi, M.; Edwards, S. F. The Theory of Polymer Dynamics; Oxford University Press: New York, 1986.
- (18) Rubinstein, M.; Colby, R. H. Polymer Physics; Oxford University Press: New York, 2003.
- (19) Shusharina, N.; Zhulina, E.; Dobrynin, A.; Rubinstein, M. Scaling theory of diblock polyampholyte solutions. *Macromolecules* **2005**, *38*, 8870–8881.

- (20) Wang, Z.; Rubinstein, M. Regimes of conformational transitions of a diblock polyampholyte. *Macromolecules* **2006**, 39, 5897–5912.
- (21) Rumyantsev, A. M.; Zhulina, E. B.; Borisov, O. V. Complex coacervate of weakly charged polyelectrolytes: Diagram of states. *Macromolecules* **2018**, *51*, 3788–3801.
- (22) Rubinstein, M.; Liao, Q.; Panyukov, S. Structure of liquid coacervates formed by oppositely charged polyelectrolytes. *Macromolecules* **2018**, *51*, 9572–9588.
- (23) Aponte-Rivera, C.; Rubinstein, M. Dynamics of liquid coacervates formed by oppositely charged polyelectrolytes. *Bull. Am. Phys. Soc.* **2019**, *64*, na.
- (24) Aponte-Rivera, C.; Rubinstein, M. Dynamics of entangled liquid coacervates made from oppositely charged polyelectrolytes. *AIChE Annual Meeting* **2019**, na.
- (25) Milner, S. T. Unified entanglement scaling for flexible, semiflexible, and stiff polymer melts and solutions. *Macromolecules* **2020**, *53*, 1314–1325.
- (26) Rubinstein, M.; Semenov, A. N. Thermoreversible gelation in solutions of associating polymers. 2. Linear dynamics. *Macromolecules* **1998**, *31*, 1386–1397.
- (27) Rubinstein, M.; Semenov, A. N. Dynamics of entangled solutions of associating polymers. *Macromolecules* **2001**, 34, 1058–1068.
- (28) Schlenoff, J. B. Site-specific perspective on interactions in polyelectrolyte complexes: Toward quantitative understanding. *J. Chem. Phys.* **2018**, 149, 163314.
- (29) Diddens, D.; Baschnagel, J.; Johner, A. Microscopic structure of compacted polyelectrolyte complexes: Insights from molecular dynamics simulations. *ACS Macro Lett.* **2019**, *8*, 123–127.
- (30) Andreev, M.; Prabhu, V. M.; Douglas, J. F.; Tirrell, M.; de Pablo, J. J. Complex coacervation in polyelectrolytes from a coarse-grained model. *Macromolecules* **2018**, *51*, *6717–6723*.
- (31) Kremer, K.; Grest, G. S. Dynamics of entangled linear polymer melts: A molecular-dynamics simulation. *J. Chem. Phys.* **1990**, 92, 5057–5086.
- (32) Likhtman, A. E.; Sukumaran, S. K.; Ramírez, J. Linear viscoelasticity from molecular dynamics simulation of entangled polymers. *Macromolecules* **2007**, *40*, 6748–6757.
- (33) Grosberg, A. Y.; Khokhlov, A. R. Statistical Physics of Macromolecules; AIP Press: New York, 1994.
- (34) Dobrynin, A. Electrostatic persistence length of semiflexible and flexible polyelectrolytes. *Macromolecules* **2005**, *38*, 9304–9314.
- (35) Auhl, R.; Everaers, R.; Grest, G. S.; Kremer, K.; Plimpton, S. J. Equilibration of long chain polymer melts in computer simulations. *J. Chem. Phys.* **2003**, *119*, 12718–12728.
- (36) Liao, Q.; Carrillo, J.-M. Y.; Dobrynin, A. V.; Rubinstein, M. Rouse dynamics of polyelectrolyte solutions: Molecular dynamics study. *Macromolecules* **2007**, *40*, 7671–7679.
- (37) Baschnagel, J.; Bennemann, C.; Paul, W.; Binder, K. Dynamics of a supercooled polymer melt above the mode-coupling critical temperature: Cage versus polymer-specific effects. *J. Phys.: Condens. Matter* **2000**, *12*, 6365–6374.
- (38) Binder, K.; Baschnagel, J.; Paul, W. Glass transition of polymer melts: Test of theoretical concepts by computer simulation. *Prog. Polym. Sci.* **2003**, *28*, 115–172.
- (39) Schweizer, K. S.; Saltzman, E. J. Theory of dynamic barriers, activated hopping, and the glass transition in polymer melts. *J. Chem. Phys.* **2004**, *121*, 1984–2000.